In Situ Chemical Transformations of Silver Nanoparticles along the Water-sediment Continuum

Author

Khaksar, Maryam, Jolley, Dianne F, Sekine, Ryo, Vasilev, Krasimir, Johannessen, Bernt, Donner, Erica, Lombi, Enzo

Published

2015

Journal Title

Environmental Science & Technology

DOI

10.1021/es504395m

In-situ chemical transformations of silver nanoparticles along the water-sediment continuum

Maryam Khaksar,[1*] Dianne F Jolley,[2] Ryo Sekine,[3] Krasimir Vasilev,[1] Bernt Johannessen,[4] Erica Donner,[3,5] and Enzo Lombi[3]

1. Mawson Institute, University of South Australia, Building V, Mawson Lakes Campus, South Australia, 5095, Australia

2. School of Chemistry, University of Wollongong, Wollongong, New South Wales 2522, Australia

3. Centre for Environmental Risk Assessment and Remediation, University of South Australia, Building X, Mawson Lakes Campus, South Australia, 5095, Australia

4. Australian Synchrotron, Clayton, Victoria 3168, Australia

5. CRC CARE, PO Box 486, Salisbury, South Australia 5106, Australia

Corresponding author: Enzo Lombi E-mail address: enzo.lombi@unisa.edu.au

Abstract

In order to accurately assess the potential environmental risk posed by silver nanoparticles (Ag-NPs), their transformation and fate must be investigated in realistic natural systems. This has proven to be very challenging due to the difficulties encountered in retrieving/analysing NPs dispersed in complex and heterogeneous environmental matrices at relevant (i.e. low) concentrations. In this study, we overcame this challenge by immobilising functionalised Ag-NPs onto plasma polymerised solid substrates to form 'nano *in situ* deployment devices' (nIDDs). This method allowed us to retrieve and analyze the Ag-NPs after 24 h of direct exposure in freshwater-sediment and saltwater-sediment environments. The type and extent of Ag-NPs transformation was expected to vary along the water-sediment continuum as sediments typically contain steep gradients in solute concentrations and redox potential. To trace the distribution of redox sensitive elements (e.g. Fe, Mn), Diffusive Equilibration in Thin-films (DET) devices were inserted into the sediments alongside the nIDDs. Chemical transformation of the immobilised Ag-NPs across the water-sediment continuum was investigated after retrieval by synchrotron radiation X-ray Absorption Spectroscopy (XAS). Linear combination fitting of Ag K-edge X-ray absorption spectra indicated that the chemical transformations of Ag-NPs in both freshwater and saltwater sediments were strongly affected by the redox conditions over the investigated range. Ag bound to reduced sulfur was the principal product of Ag-NP transformations but different extents of transformation were observed for Ag-NPs exposed to different depths in the sediment. These field results add important insights about the transformation of Ag-NPs in heterogeneous environments.

Introduction

Engineered silver nanoparticles (Ag-NPs) have attracted substantial attention over the last two decades and are now used in a variety of applications ranging from electronics to biomedical devices [1-4] and water purification [5]. They are also utilized in a large number of products from home appliances and textiles [6] to personal care products[4]. Consequently, concerns have been raised about the potential for environmental impacts to occur as a result of exposure to silver nanoparticles and ionic silver, both of which may be released from these products [7].

Once released to the environment, Ag-NPs are subject to complex chemical, physical [8] and biological [9] transformation processes which may alter their physicochemical properties and complicate their accurate environmental risk assessment [10, 11]. Many factors determine the fate, stability and bioavailability of Ag-NPs in the environment including their particle size, surface charge [12, 13], aggregation state and dissolution rate [14], as well as the characteristics of the receiving medium such as the pH, ionic strength [15], dissolved oxygen, redox potential [16] and presence of natural organic matter [14, 17]. Among the challenges encountered in assessing the fate of nanoparticles in the environment, the lack of adequate methodologies for detection, retrieval and quantification of nanoparticles dispersed in complex and heterogeneous environmental matrices at environmentally relevant concentrations remains a serious constraint [18]. For these reasons most nanoparticle fate experiments conducted to date have been laboratory-based. There have however been increasing efforts to generate data from more realistic exposure scenarios, and a few studies have been recently performed using mesocosms. For instance, Lowry et al. [19] used a mesocosm simulating freshwater emergent wetlands to investigate the long-term transformation of Ag-NPs, and found silver sulfide and cysteine-bound silver to be the dominant species in the exposed soil and subaquatic sediments. These results were representative of the average Ag speciation in discrete compartments within the mesocosms (i.e. homogenised samples from the top 1 cm of the soil and sediment). Results from these experiments provide valuable information about potential

nanoparticle fate but are still limited in some respects and may not directly extrapolate to a full understanding of nanoparticle transformations under realistic environmental conditions where exposures will likely be at low concentrations and could be affected by a diversity of organisms. However, field experiments are complicated and costly, and extremely difficult to conduct at relevant concentrations. To our knowledge, the only ongoing field experiment is the LENS (Lake Ecosystem Nanosilver) project [20] in which Ag-NPs are being released to the Experimental Lakes Area in Ontario, Canada, to monitor the transformation and spatial movement of nanosilver within a natural lake ecosystem. This is a very valuable study but cannot be replicated at many sites. Clearly, innovative and practical approaches that enhance our ability to assess the transformation and fate of nanoparticles in natural environments are required.

The water-sediment continuum is a good example of a highly complex and heterogeneous natural environment in which matrix composition and redox conditions vary over small distances. Due to the presence of significant gradients in solute concentrations and redox potential [21], important Ag-NP transformation reactions such as oxidation [22] and sulfidation [23] are also expected to differ in relevance and intensity across this continuum. For instance, under oxic conditions Ag-NPs may undergo oxidative dissolution, whilst in the presence of inorganic ligands they may partially/fully transform to silver sulfide or silver chloride. This could translate into a significant decrease in bioavailability and toxicity due to the low solubility of these compounds [11].

To help elucidate the *in situ* chemical transformation of Ag-NPs in heterogeneous natural environments we applied a novel approach that was recently developed by our team [24], namely the use of nano *in situ* deployment devices (nIDDs). After plasma polymerising a solid substrate with a suitably charged coating, functionalised nanoparticles can be immobilised on the substrate surface to produce a nIDD [24]. These devices can be deployed directly into natural environmental systems for nanoparticle transformation experiments and just as readily retrieved again following exposure. In the study described here, nIDDs were used to conduct a spatially resolved investigation of Ag-NP

transformation reactions upon exposure to complex natural water-sediment environments. Ag-NPs engineered with two different capping agents (i.e. polyethyleneglycol (PEG) and citrate) were immobilized onto large (13.9 x 1.9 cm) plasma polymerized substrates. These devices were partially inserted into freshwater and seawater sediments. To spatially resolve the concentration of redox-sensitive elements (e.g. Fe, Mn) across the water-sediment continuum, diffusive equilibrium in thin film (DET) devices were inserted into the sediments alongside the substrates. Following retrieval, DET gel slices were excised from the constrained probe, equilibrated into acid, and used to determine the concentrations of redox sensitive elements across the sediment-water interface, while the nIDDs retrieved from the same sites were analysed using Ag K-edge X-ray Absorption Near Edge Structure (XANES) spectroscopy to investigate the chemical transformation profiles of the immobilised Ag-NPs. The primary objectives for this study were to determine the short term transformation of Ag-NPs in a realistic and complex saltwater and freshwater sediments, and to correlate the redox condition of the environmental compartments with the observed speciation. The effect of various processes on the biogeochemical cycling of redox sensitive elements and the differences between a static and tidally driven redox environments and its effect on Ag speciation are discussed.

Materials and methods

Preparation of Ag-NPs suspensions. Ag-NPs were prepared using a chemical reduction method. A 1 mM silver nitrate solution ($AgNO_3$, Sigma Aldrich, 99.99 %) was reduced by dropwise addition of 2 mM sodium borohydride ($NaBH_4$, Sigma Aldrich, 98%). The solution was stirred vigorously throughout and turned yellow indicating the formation of Ag-NPs. Two different capping agents were used to stabilize the NP suspensions: trisodium citrate ($Na_3C_3H_5O(COO)_3$, Ajax Finechem, 99%)

or polyethyleneglycol (PEG, MW_{av}=6000 g/mol, Technical grade, VWR). This procedure was followed by an additional 1 h of stirring at 100 ºC. The suspensions were then removed from the heating plates and stirred for a further 30 minutes. The pH of the final product was 8.1 for citrate-Ag-NPs and 8.5 for PEG-Ag-NPs. These aqueous colloidal Ag-NPs are stable for several months when sealed and stored in dark, indicating good stabilization of Ag-NPs due to the adsorbed monolayer of citrate and PEG on the nanoparticles' surface.

The particle size distribution and surface charge of PEG/citrate-Ag-NPs suspended in MiliQ water (18.2 MΩ) was measured by Dynamic Light Scattering (DLS) using a Nicomp 380 ZLS (Particle Sizing Systems, FL, USA). PEG/citrate-Ag-NPs had an average (number weighted) hydrodynamic diameter of 20 nm (Figure S1 and S2 of Supporting Information (SI)) and ζ-potentials of -30 mV and -33 mV, respectively.

Immobilization of Ag-NPs. Immobilisation of Ag-NPs was conducted as described previously [3, 24]. Perspex (2 mm thick) was cut into rectangular pieces (139×19 mm) with an internal window of 125×6 mm (Figure S3 in SI). Both sides of this frame were covered with a 63.5 µm thick adhesive polyimide tape (2.5 mil, Cole-Palmer, EW- 08277-82). All the substrates were cleaned with ethanol before plasma polymer coating. Plasma polymerisation was conducted on one side of the devices using a custom-built parallel plate plasma reactor [24] and a 13.56 MHz plasma generator to introduce suitable functional groups onto the surfaces. Before plasma coating, all substrates were cleaned by oxygen plasma for 2 minutes using a power of 40 W at a pressure of 2×10^{-1} mbar. Surfaces carrying positive charges were prepared using allylamine as a precursor for plasma polymerisation with this reaction taking place over a period of 2 minutes, with 40 W power and 2×10^{-1} mbar pressure. These conditions resulted in the deposition of an amine-functionalized coating about 25 nm thick, as measured by ellipsometry. Immobilisation of nanoparticles was carried out by immersing the plasma polymer coated substrates in a solution of nanoparticles for 24 h. The negatively charged

PEG/citrate-Ag-NPs were electrostatically bound to the positively charged polyallylamine. The immobilisation step was followed by triple rinsing with Milli-Q water to remove all weakly bound nanoparticles. All the samples were kept under an argon atmosphere until deployment. The devices produced via this process are referred to as nIDDs (nano in situ deployment devices).

Characterisation of the devices. Three Si wafer substrates (1 × 1 cm) were placed alongside the large nIDDs substrates during the polymerisation process and underwent the same Ag-NP immobilization process. The distribution, size and morphology of Ag-NPs immobilized on the Si substrates were assessed using a Scanning Electron Microscope (SEM, FEI Quanta 450 FEG-ESEM) equipped with an Energy Dispersive X-ray (EDX) spectrometer (EDAX Apollo X). This quality control step was conducted on Si substrates as they are well suited to SEM analysis (whereas the polyimide surface used for the field deployed nIDDs is ideal for XANES analysis). The SEM was operated using an acceleration voltage of 20 kV and images were collected in both backscattered (BSE) and secondary electron (SE) modes. The size distribution of the attached NPs was assessed using ImageJ software [25]. Furthermore, X-ray Photoelectron Spectroscopy (XPS) was used to investigate the surface composition of the substrates. XPS spectra were collected from the substrates using a SPECS SAGE spectrometer with an Mg Kα radiation source ($h\nu$ = 1253.6 eV) operating at 10 kV and 20 mA.

Field deployment of nIDDs and DET probes. The nIDDs with two differently-coated Ag-NPs were deployed in two different locations; one freshwater pond at the University of Wollongong and one marine lake (Lake Illawarra, New South Wales) for 24 h. Approximately 10 cm of each device was inserted into the sediment leaving 2 cm in the overlying water. It should be noted that a significant storm and local flooding occurred during the field experiment. After retrieval, nIDDs were thoroughly rinsed, dried and stored under nitrogen at 4 °C to prevent further transformations before

speciation analysis. Constrained Diffusive Equilibrium in Thin Films (DET) sediment probes were purchased from DGT Research Ltd (Lancaster, UK), and set with agarose [26], conditioned and deoxygenated before deployment. All gel preparations and probe manipulations were performed in an AURA SD4 Laminar Flow Cabinet. The DET probes were inserted in sediment alongside the substrates for 24 h. Upon retrieval, probes were thoroughly rinsed with Milli-Q water and stored separately with 1 mL of Milli-Q water at 4 ºC until processed for analysis. DET gel slices were excised from the probe and re-equilibrated in ≥ 0.1 M HNO_3 for 24 h with gentle agitation and the gel removed prior to analysis. Metal analyses were performed by inductively coupled plasma-mass spectrometry (ICP-MS) using an Agilent 7500ce (utilising both standard and collision/reaction gas modes). Extra (undeployed) DET probes were analyzed as handling blanks and their metal concentrations were confirmed to be less than 5% of the lowest measured concentration. As part of the quality assurance, analyses of filter and acid-digest blanks, replicates for 20% of samples, and analyte sample-spikes were performed.

Salinity measurements were performed using a WTW meter (LF 320) with a Tetra-Con 325 probe. A Sensorex combination pH electrode (450C) with a Rex pH meter (Model pHb-4) was used for all pH measurements and was calibrated against standardised pH 4 and pH 7 NIST buffers before use [27]. Total organic carbon (TOC) analyses in sediments were made using a high temperature TOC analyser (Dohrmann DC-190) following the removal of inorganic carbon (carbonates and bicarbonates) by acidification with 1 M HCl until effervescence was completed. Sediment particle size fractionation was made by wet sieving the sediments through 180 and 63 µm mesh [27]. Acid-volatile sulfide measurements were made on subsamples of the homogenized sediment under nitrogen atmosphere [28].

X-ray Absorption Spectroscopy. The chemical speciation of Ag on the field deployed nIDDs was determined by X-ray Absorption Near Edge Structure (XANES) spectroscopy. Ag K-edge X-ray

absorption spectra were collected at the XAS beamline at the Australian Synchrotron (AS), Clayton, Victoria. The electron storage ring operated at 3 GeV in top-up mode. A liquid nitrogen-cooled Si (311) crystal monochromator was used to select the incident photon energy. The spectrum of a metallic Ag foil was collected in transmission mode congruently with each sample scan, and all spectra were calibrated using the first inflection point (25514 eV) of the Ag foil K-edge spectra. Spectra of the samples were recorded in fluorescence mode with a 100-element Ge detector array placed at 90^{o} to the incident beam. XANES spectra were collected at room temperature from at least thirteen positions from each device (i.e. every 10 mm), representing different depths along the water-sediment continuum. Additional spectra were collected where a notable change was observed. Reference spectra were collected at the same beamline at room temperature using the following Ag standards (diluted in cellulose for fluorescence detection): PEG/citrate-Ag-NP control, silver-oxide (Ag_2O), silver-sulfide (Ag_2S), silver-carbonate (Ag_2CO_3), and silver-phosphate (Ag_3PO_4), as well as Ag sorbed to SRfulvic (Suwannee River fulvic acid, purchased from the International Humic Substances Society (IHSS)), and Ag sorbed to cysteine and acetate. Silver-chloride (AgCl), silver-sulfate (Ag_2SO_4), and Ag sorbed to ferrihydrite and to cystine were collected at the Advanced Photon Source (APS) at the Argonne National Laboratory (ANL), U.S.A (Figure S4 in SI). Principal component analysis (PCA) of the normalised sample spectra was used to estimate the likely number of species contributing to the overall spectra and target transformation (TT) was used to identify relevant standards to use for Linear Combination Fitting (LCF). PCA and TT were performed using the SixPack program [29] and the XANES spectra were analysed by LCF using the Athena software [30]. The normalized spectra were fitted in the range of −50 to +100 eV from the absorption edge and a combination of up to 5 standards was used.

Results and discussion

Characterization of the nIDDs and sediments

SEM analysis of the nIDDs revealed that PEG/citrate-Ag-NPs were successfully immobilized on the plasma polymerised substrates (Figure 1; Si substrates). The NPs were uniformly dispersed without notable aggregation. The average size of the NPs determined using ImageJ was 18 nm (Figures S1 and S2 of SI). The surface chemistry of the nIDDs was assessed by XPS (Figure S5) and showed ca. 7 % Ag (at. %) on both the citrate and PEG capped nanoparticle substrates. The variability in Ag coverage on three replicate Si substrates was small (< 8 % for each coating), indicating that the nanoparticles were uniformly distributed across the nIDD surfaces.

Physical and chemical characteristics of the bulk freshwater and saltwater sediments (moisture content, particle size, TOC, AVS and pH) are summarized in Table 1. The pH was 7.2 ± 0.1 for the saltwater sediment and 7.5 ± 0.2 for the freshwater sediment. TOC and AVS content were greater in the saltwater sediment (%TOC = 27 ± 4; AVS = 4.4 ± 1.5 μmol/g) than in the freshwater sediment (%TOC = 17 ± 6; AVS = 0.8 ± 0.3 μmol/g).

Silver, iron and manganese chemistry in saltwater sediment

In the saltwater environment there was a visible fluffy layer on the sediment surface. This layer was assumed to be sediment and light organic matter, as the deployment zone was adjacent to a seagrass bed that contained fragments of *Zostera capricornia* at various levels of degradation and some clumping algae. The sediment was high in organic carbon (27 $\pm$ 4%), had a pH of 7.2 $\pm$ 0.1, and a temperature of 18 °C (Table 1). There were also visible amphipods and their burrows on the sediment surface.

XANES spectra collected from the PEG-Ag-NP nIDDs (Figure 2B) and associated Linear Combination Fitting (LCF) results (Figure 3C; Table S1 in SI) indicated that at the SWI and in the sediments below a substantial proportion of Ag was associated with reduced S. Although the Ag speciation from the

SWI to 20 mm below the sediment surface was dominated by complexation with reduced S, the analysis of several points on the nIDD in close proximity to one another (i.e. -10, -12.5, -17.5, -20, and -25 mm below the SWI) revealed a substantial heterogeneity in Ag speciation. Also the DET profiles indicated the elevated concentrations of dissolved Mn and Fe above the sediment-water interface (SWI) (Figures 3A and 3B). These findings indicate that the redox environment was highly heterogeneous in this dynamic and organic-rich region. Biogeochemical studies on sedimentary S cycling [31, 32] suggest that sulfate reduction carried out by anaerobic bacteria results in the accumulation of organosulfur (thiol) ligands in sedimentary organic matter. Therefore, Ag-NPs exposed in the top part of the sediments may have been complexed by reduced S ligands (e.g cysteine-bound Ag). XANES analysis does not allow an unequivocal assessment of the exact contribution of Ag complexed to thiol species (e g. Ag-cysteine) and Ag_2S as these two species have similar XANES spectra (Figure S6A in SI). However, Ag_2S and Ag-cysteine can be differentiated in k-space in the Extended X-ray Absorption Fine Structure (EXAFS) range (Figure S6B of SI). On plotting the sample spectra in k-space and comparing against the Ag_2S and Ag-cysteine reference spectra it is apparent that Ag_2S is the dominant species of Ag in the top layer of the sediments (Figure S6C in SI). However, as the data in k-space are relatively noisy and the XANES spectra for Ag_2S and Ag-cysteine are not easily distinguishable, their LCF percentage contributions to the sample spectra are combined in Table S1 and S2 of the SI as Ag bound to reduced S. Sulfide production via sulfate microbial reduction usually does not take place near the SWI and occurs in deeper layers in sediments when the supply of other electron acceptors (e.g. Fe(III) and Mn(IV)) are exhausted.

It should be considered that Lake Illawara is technically a saline estuary and it has been well documented that coastal sediments are influenced by tidal forcing which has an important effect on biogeochemical cycling of reduced sulfur and redox sensitive metals as Mn and Fe [33-35]. Hence, distribution of redox chemical species in first few centimetres near the SWI is expected to be distinctively different from static redox environments. Given that nIDD and DET probe were deployed in saltwater sediment for 24 hours, this suggests that they were subject to two tide cycles.

Under the influence of the tidal changes and the steep gradient in hydrostatic pressures between high and low tide, dissolved sulfide can be displaced from deeper in the sediment to the surface [36]. This increase in dissolved sulfide concentration is likely results in greater extent of Ag-NP sulfidation as observed near the SWI in the nIDDs XANES data. Concurrently, this displacement of dissolved sulfide towards the SWI can be expected to result in a decrease in dissolved Fe by precipitation of Fe to its sulfidized form. However, this is contrary to the DET data where an increase is observed towards the SWI. Therefore, elevated concentration of Fe near the SWI with large content of dissolved sulfide indicates that another Fe reduction process must be dominant in this region such as microbial reduction of iron oxides near the SWI [37]. Also according to thermodynamic considerations, the reduction of Fe(III) via oxidation of FeS_2 or FeS occur in the presence of H_2O and without the necessity for O_2 as an initiation agent. These processes would prevent the depletion of the Fe(II) pool in this region [38]

Bioturbation in sediments could be another factor that increases the permeability and facilitate the oxygenation of the top few centimetre of the sediment which result in Fe(II) removal via production of iron oxides and affects the geochemical cycling of Fe. Therefore, it can be concluded that water transportation during the tide cycles is not the only effective factor and combination of physical, geochemical and biological factors are influencing the distribution of redox sensitive elements in surficial sediments. However, previous studies [33] suggested that bioturbation is less effective in changing the sediment redox conditions and tidal dynamics and biological factors has the most profound effect on chemistry of the system.

Therefore, DET data in this study indicates the time averaged distribution of dissolved Fe and Mn over the 24h deployment. This is in line with previous studies where the concentration of Fe and dissolved sulfide have been found to reach to their maximum in near the SWI measured in one tide cycle [36].

Deeper layers in the sediment are expected to be less influenced by tidal fluctuations because of the decrease in porosity and permeability [36]. In this study, the saltwater sediments were highly silty

(particle size analysis: 82 % in the <63 µm fraction; 2% in the 63-180 µm fraction; and 16% in the >180 µm fraction), ensuring that below (<-30 mm) the sediments were very compact and less permeability of sediment restricts the tidal effects on chemical composition of the sediment. The decrease in porewater Fe(II) occurred in two steps, a rapid depletion started at ~20 mm coincident with Mn(II) decrease, and again at ~62 mm. It is likely that this second region demarcated the sub-oxic/anoxic interface, where sulfides become labile within porewaters, as it is supported by an almost complete sulfidation of Ag (Table S3 of the SI; which is also confirmed by Figure S6D). The saltwater sediment had a high acid volatile sulfide (AVS) concentration (4.4 $\pm$ 1.5 µmol/g AVS), confirming that sulfide was not limiting in this environment.

Comparable sulfidation trends were observed for citrate-Ag-NPs exposed to saltwater sediments (Figure S7, S8 and Table S3 of the SI), with an additional minor contribution of Ag bound to organic matter (Ag-SRFA standard) indicated by LCF for the citrate-Ag-NPs exposed to saltwater sediments.

Silver, iron and manganese chemistry in freshwater sediment

In the freshwater study, the nIDDs and DET probes were deployed approximately 0.5 m away from fringing plants in sediments with no visible indicators of disturbance, pH 7.5 $\pm$ 0.2, and temperature ~13 °C (Table 1). The sediment was a compact silty-sand (52, 21, 27% as <63, 63-180, >180 um particle sizes), with a relatively high organic carbon content (17 $\pm$ 6%).

The Ag XANES spectra from the PEG-Ag-NP nIDD exposed to the freshwater environment are presented in Figure 2A. Visual inspection of all spectra immediately suggests that there are notable changes in spectral patterns along the water-sediment continuum. Similarly, the concentration of Fe and Mn in the DET follows a complex pattern, which reflects the redox conditions in the sediments (Figure 4A, B). The concentrations of both Fe and Mn are low in the water column (column of water from the surface of the lake to the surface of sediment) as is expected under oxic

conditions. XANES analysis reveals that the PEG-Ag-NPs exposed in the water column are almost unchanged upon retrieval, with the LCF fitting showing that most of the Ag remains in the metallic form (Table 2 and Figure 4C). A low proportion of Ag was found to be associated with reduced S species (Table 2 in SI). Sekine et al. [24] reported a larger degree of association with reduced S species for PEG-Ag-NPs exposed to freshwater conditions. However, in that case the deployment time was longer (48 h) and the lake, which forms part of a recycled water circulation system, contained large concentrations of organic matter and consequently reduced organic S species. Sulfide concentration in oxic water is generally very low; usually in the µg/L levels [39, 40]. Sulfate is the predominant inorganic S in oxygenated waters and no reaction is expected between Ag-NPs and sulfate [41].

The reduction of Fe and Mn (oxyhydr)oxides delineates the redox boundary between oxic and sub-oxic sediments, that is, the boundary where the electron acceptors with positive pε levels are no longer the primary acceptors [42, 43]. This boundary occurred just below the SWI as shown by the rapid increase in the DET concentrations of dissolved Mn and Fe (Figure 4A, B). Below this boundary, Fe(II) is most likely being produced by dissimilatory reduction of Fe(III) oxides, as near the sediment surface there is more organic C and more bioavailable Fe(III) oxides [44, 45]. This causes relatively fast reductive dissolution of Fe(III) oxides and the ongoing formation of sufficient Fe(II), which is consistent with the accumulation of porewater Fe(II) observed in this region. Congruently, under these mild reducing conditions the percentage of nIDDs Ag bound to reduced S increases in this sediment region to approximately 10-20% (Table 2). Both thermodynamic calculations and experimental data suggest that sulfidized silver is the favoured chemical form of silver at typical environmental sulfide concentrations [11, 19]. As silver has high affinity for reduced sulfur and Ag_2S has very low solubility ($K_{sp} = 6 \times 10^{-51}$) and high stability, silver sulfide is expected to be the ultimate form of silver in natural environment.

The decrease of Fe(II) in the porewaters at depths >35 mm is the result of sulfate reduction which subsequently causes the precipitation of iron-sulfides [46, 47]. Dissolved Mn continued to increase, peaking at 60 mm depth, which was also the depth at which the Fe(II) decreased to concentrations similar to those at the SWI. This identified the sub-oxic:anoxic interface within the sediments. At intermediate depths (but still above the region of porewater sulfide production), there is less available organic C and less Fe(III) oxides, meaning that Fe(II) is produced at a rate that is less than its rate of removal. The Fe(II) removal processes would include diffusion upwards towards the SWI and downwards in the profile, and the precipitation of Fe(II)-bearing minerals [43]. These minerals could include siderite, green-rusts or iron sulfides (including pyrite, which requires the partial oxidation of S^{2-}) [48]. Although one possibility for iron sulfidation is formation of FeS by reaction between dissolved Fe(II) and limited available sulfide, FeS is generally replaced by stable Fe-disulfides (e.g pyrite and marcasite) via abiotic and microbially mediated reactions. From a kinetic perspective, pyrite formation occurs faster in sediment layers where the produced S^{2-} is being oxidised to S^{-} in polysulfides. This is consistent with an intermediate depth where Fe(II) and S^{2-} exist only at very low concentrations. At greater depth, the bioavailable Fe(III) pool becomes exhausted thereby allowing a major "regime-shift" in terms of the dominant terminal electron accepting process. That is, sulfate-reduction becomes dominant. Porewater S^{2-} accumulates because there is no available Fe(III) oxides to react with (i.e. forming S^{0} or S^{-}) and no porewater Fe(II) (due to fast precipitation of FeS and the absence of Fe(III) oxides). Sulfide was present at relatively low concentrations (0.8 $\pm$ 0.3 µmol/g AVS) in the sediment, and the accumulation of porewater sulfide at sediment depths > 60 mm was evident by the dominance of Ag-sulfides on the nIDD (Figure 4C and Table S2 in SI). These results are consistent with previous studies [41] where a greater extent of silver sulfidation was observed when the available sulfide concentration was elevated in the system. It is unlikely that pyrite is contributing to the Ag_2S formation on the probe, as pyrite has very low solubility (thus slow dissolution), is kinetically stable, and contains S^{-}.

No transformation was observed for citrate-Ag-NPs deployed in freshwater sediments. It is suspected that the nIDD may have become displaced during deployment as this coincided with a significant weather change and local flooding.

To investigate the potential loss of Ag-NPs from the nIDDs over the course of deployment, the amount of Ag on the nIDDs surfaces was examined after retrieval (figure S9 in SI). Normalised X-Ray Fluorescence (XRF) intensity from the samples after exposure showed some loss of Ag from the PEG-Ag-NP nIDDs, but a higher extent of Ag loss was observed for citrate-Ag-NPs exposed to oxic water. This may be attributed to the higher stability of the PEG-Ag-NPs. PEG has a higher affinity to the Ag surface than citrate, and the latter is more easily displaced by other molecules from the surrounding environment. This could likely lead to a faster rate of dissolution of citrate-Ag-NPs than PEG-Ag-NPs. Steric factors may also play a role in PEG-AgNPs, potentially inhibiting reactive species from reaching the Ag surface. A higher Ag loss was also observed for citrate-Ag-NP deeper within the sediments (both for freshwater and saltwater nIDDs). Microbial biodegradation of citrate by anaerobic bacteria (sulfate/iron reducing bacteria) may have led to increased dissolution of citrate-Ag-NPs within these sediment layers [49, 50]. Another possible reason could be abrasion and physical detachment of Ag-NPs from the surface while inserting the nIDD into the sediment because of the more compact texture of sediment in deeper area.

This study confirmed the feasibility of the use of nIDDs for investigating the chemical transformation of Ag-NPs *in situ*. In comparison to the study reported by Sekine et al [24], where much smaller devices (25 × 8 mm) were used to determine the average Ag-NP transformation chemistry in aquatic exposure environments, this study demonstrates that nIDDs can be also used to explore highly dynamic and spatially heterogeneous environments by using a larger device that can extend across interfaces and be used to obtain spatially resolved chemical speciation data. The current study, which investigated two soil-sediment continua, revealed a very complex transformation pattern for Ag-NPs within a few centimetres from the sediment surface. Our results indicate that Ag speciation

is highly affected by chemical mobility in different redox zones, which can be caused by tidal fluctuations, biological and physical properties of the sediment at the SWI. As Ag speciation strongly influences its bioavailability, the toxicity of Ag to organisms that inhabit different sediment layers can vary greatly [51]. This addresses the necessity for investigating the transformation and fate of nanomaterials under more realistic environmental conditions. The use of nIDD provides an easy approach to monitor the complex behaviour of Ag NPs (or other classes of ENPs) where laboratory based experiments cannot capture the complexity and dynamic nature of real environments. Given the profound impact of tidal forces on Ag speciation, in situ time series measurement of Ag speciation and redox biogeochemical properties of sediment during tidal cycles at water sediment continuum will be incorporated in future studies.

Acknowledgements

E.L., K.V., and E.D., are recipients of Australian Research Council Future Fellowships FT100100337, FT100100292, and FT130101003 respectively. The funding support from the Australian Research Council Discovery Project DP120101115 is gratefully acknowledged. This research was undertaken on the XAS beamline at the Australian Synchrotron, Victoria, Australia. We thank Dr Rachel Popelka-Filcoff for help in procuring the frames for the nIDDs, Mr. Marc Long for his help in physical characterization of the sediment and Mr Stuart McClure for his support on SEM analysis.

Supporting information

Supporting information includes: Particle Size Distribution (PSD) histograms; DLS size distributions; XPS spectra; XRF intensity measurements; XANES spectra of all Ag standards used in the LCF procedure; EXAFS analysis of the sample spectra; Ag K-edge XANES spectra of the citrate-Ag-NPs exposed to the saltwater-sediment; depth profile of citrate-Ag-NPs speciation in saltwater-sediment;

Schematic and photo of XAS substrate; LCF results of the Ag K-edge XANES spectra of PEG-Ag-NPs exposed to saltwater/freshwater sediments; LCF results of the Ag K-edge XANES spectra of citrate-Ag-NPs exposed to saltwater sediments; and DET data for saltwater/freshwater sediments. This information is available free of charge via the Internet at http://pubs.acs.org/.

References

1. Chernousova, S. and M. Epple, *Silver as Antibacterial Agent: Ion, Nanoparticle, and Metal.* Angewandte Chemie-International Edition, 2013. **52**(6): p. 1636-1653.
2. Taheri, S., et al., *Substrate independent silver nanoparticle based antibacterial coatings.* Biomaterials, 2014. **35**(16): p. 4601-4609.
3. Vasilev, K., et al., *Antibacterial surfaces by adsorptive binding of polyvinyl-sulphonate-stabilized silver nanoparticles.* Nanotechnology, 2010. **21**(21).
4. *The Project on Emerging Nanotechnologies. http://www.nanotechproject.org/.*
5. Kiruba, V.S.A., A. Dakshinamurthy, and P.M. Selvakumar, *Eco-Friendly Biocidal Silver-Activated Charcoal Nanocomposite: Antimicrobial Application in Water Purification.* Synthesis and Reactivity in Inorganic Metal-Organic and Nano-Metal Chemistry, 2013. **43**(8): p. 1068-1072.
6. Benn, T.M. and P. Westerhoff, *Nanoparticle silver released into water from commercially available sock fabrics.* Environmental science & technology, 2008. **42**(11): p. 4133-4139.
7. Gottschalk, F., T. Sun, and B. Nowack, *Environmental concentrations of engineered nanomaterials: Review of modeling and analytical studies.* Environmental Pollution, 2013. **181**: p. 287-300.
8. Bone, A.J., et al., *Biotic and Abiotic Interactions in Aquatic Microcosms Determine Fate and Toxicity of Ag Nanoparticles: Part 2-Toxicity and Ag Speciation.* Environmental Science & Technology, 2012. **46**(13): p. 6925-6933.
9. Kirschling, T.L., et al., *Microbial Bioavailability of Covalently Bound Polymer Coatings on Model Engineered Nanomaterials.* Environmental Science & Technology, 2011. **45**(12): p. 5253-5259.
10. Lowry, G.V., et al., *Transformations of Nanomaterials in the Environment.* Environmental Science & Technology, 2012. **46**(13): p. 6893-6899.
11. Levard, C., et al., *Environmental Transformations of Silver Nanoparticles: Impact on Stability and Toxicity.* Environmental Science & Technology, 2012. **46**(13): p. 6900-6914.
12. Tejamaya, M., et al., *Stability of Citrate, PVP, and PEG Coated Silver Nanoparticles in Ecotoxicology Media.* Environmental Science & Technology, 2012. **46**(13): p. 7011-7017.
13. El Badawy, A.M., et al., *Surface Charge-Dependent Toxicity of Silver Nanoparticles.* Environmental science & technology, 2011. **45**(1): p. 283-287.
14. Fabrega, J., et al., *Silver nanoparticles: Behaviour and effects in the aquatic environment.* Environment International, 2011. **37**(2): p. 517-531.
15. Levard, C., et al., *Effect of Chloride on the Dissolution Rate of Silver Nanoparticles and Toxicity to E. coli.* Environmental science & technology, 2013. **47**(11): p. 5738-5745.
16. Dale, A.L., G.V. Lowry, and E.A. Casman, *Modeling Nanosilver Transformations in Freshwater Sediments.* Environmental science & technology, 2013. **47**(22): p. 12920-12928.

17. Angel, B.M., et al., *The impact of size on the fate and toxicity of nanoparticulate silver in aquatic systems.* Chemosphere, 2013. **93**(2): p. 359-65.
18. Howard, A.G., *On the challenge of quantifying man-made nanoparticles in the aquatic environment.* Journal of Environmental Monitoring, 2010. **12**(1): p. 135-142.
19. Lowry, G.V., et al., *Long-Term Transformation and Fate of Manufactured Ag Nanoparticles in a Simulated Large Scale Freshwater Emergent Wetland.* Environmental Science & Technology, 2012. **46**(13): p. 7027-7036.
20. *http://www.trentu.ca/iws/lens.php*.
21. Qian, Q., V. Voller, and H.G. Stefan, *Modeling of solute transport into sub-aqueous sediments.* Applied Mathematical Modelling, 2007. **31**(8): p. 1461-1478.
22. Metz, K.M., et al., *Engineered Nanomaterial Transformation under Oxidative Environmental Conditions: Development of an in vitro Biomimetic Assay.* Environmental science & technology, 2009. **43**(5): p. 1598-1604.
23. Levard, C., et al., *Sulfidation processes of PVP-coated silver nanoparticles in aqueous solution: impact on dissolution rate.* Environmental science & technology, 2011. **45**(12): p. 5260-5266.
24. Sekine, R., et al., *Surface Immobilisation of Engineered Nanomaterials for in-situ Study of their Environmental Transformations and Fate.* Environmental science & technology, 2013.
25. Rasband, W.S.I., U.S. National Institutes of Health: Bethesda, Maryland, USA, 1997>26 and 2012.
26. Docekalova, H., et al., *Use of constrained DET probe for a high-resolution determination of metals and anions distribution in the sediment pore water.* Talanta, 2002. **57**(1): p. 145-155.
27. Li, H., et al., *Effect of pH, Temperature, Dissolved Oxygen, and Flow Rate of Overlying Water on Heavy Metals Release from Storm Sewer Sediments.* Journal of Chemistry, 2013.
28. Simpson, S.L., *A rapid screening method for acid-volatile sulfide in sediments.* Environmental Toxicology and Chemistry, 2001. **20**(12): p. 2657-2661.
29. Webb, S.M., *SIXpack: a graphical user interface for XAS analysis using IFEFFIT.* Physica Scripta, 2005. **T115**: p. 1011-1014.
30. Ravel, B. and M. Newville, *ATHENA, ARTEMIS, HEPHAESTUS: data analysis for X-ray absorption spectroscopy using IFEFFIT.* Journal of Synchrotron Radiation, 2005. **12**: p. 537-541.
31. Padmos, J.D. and P. Zhang, *Surface Structure of Organosulfur Stabilized Silver Nanoparticles Studied with X-ray Absorption Spectroscopy.* Journal of Physical Chemistry C, 2012. **116**(43): p. 23094-23101.
32. Bell, R.A. and J.R. Kramer, *Structural chemistry and geochemistry of silver-sulfur compounds: Critical review.* Environmental Toxicology and Chemistry, 1999. **18**(1): p. 9-22.
33. Luther, G.W., et al., *TEMPORAL AND SPATIAL VARIABILITY OF REDUCED SULFUR SPECIES (FES2,S2O32-) AND POREWATER PARAMETERS IN SALT-MARSH SEDIMENTS.* Biogeochemistry, 1991. **14**(1): p. 57-88.
34. Robinson, C., L. Li, and D.A. Barry, *Effect of tidal forcing on a subterranean estuary.* Advances in Water Resources, 2007. **30**(4): p. 851-865.
35. Moore, W.S., *The Effect of Submarine Groundwater Discharge on the Ocean.* Annual Review of Marine Science, 2010. **2**: p. 59-88.
36. Taillefert, M., S. Neuhuber, and G. Bristow, *The effect of tidal forcing on biogeochemical processes in intertidal salt marsh sediments.* Geochemical Transactions, 2007. **8**.
37. Zonneveld, K.A.F., et al., *Selective preservation of organic matter in marine environments; processes and impact on the sedimentary record.* Biogeosciences, 2010. **7**(2): p. 483-511.
38. Schippers, A. and B.B. Jorgensen, *Biogeochemistry of pyrite and iron sulfide oxidation in marine sediments.* Geochimica Et Cosmochimica Acta, 2002. **66**(1): p. 85-92.
39. Luther, G.W. and E. Tsamakis, *CONCENTRATION AND FORM OF DISSOLVED SULFIDE IN THE OXIC WATER COLUMN OF THE OCEAN.* Marine Chemistry, 1989. **27**(3-4): p. 165-177.

40. Tang, D.G. and P.H. Santschi, *Sensitive determination of dissolved sulfide in estuarine water by solid-phase extraction and high-performance liquid chromatography of methylene blue.* Journal of Chromatography A, 2000. **883**(1-2): p. 305-309.
41. Liu, J., K.G. Pennell, and R.H. Hurt, *Kinetics and mechanisms of nanosilver oxysulfidation.* Environmental science & technology, 2011. **45**(17): p. 7345-7353.
42. Froelich, P.N., et al., *Early diagenesis of organic matter in pelagic sediments of the eastern equatorial Atlantic: suboxic diagenesis.* Geochim. Cosmochim. Acta, 1979. **43**(7): p. 1075-1090.
43. Stumm, W. and J.J. Morgan, *Aquatic chemistry: Chemical equilibria and rates in natural waters*. 3rd ed. 1996, New York, NY: John Wiley and Sons.
44. Weber, K.A., L.A. Achenbach, and J.D. Coates, *Microorganisms pumping iron: anaerobic microbial iron oxidation and reduction.* Nature Reviews Microbiology, 2006. **4**(10): p. 752-764.
45. Roden, E.E. and R.G. Wetzel, *Kinetics of microbial Fe(III) oxide reduction in freshwater wetland sediments.* Limnology and Oceanography, 2002. **47**(1): p. 198-211.
46. Azzoni, R., G. Giordani, and P. Viaroli, *Iron-sulphur-phosphorus interactions: implications for sediment buffering capacity in a mediterranean eutrophic lagoon (Sacca di Goro, Italy).* Hydrobiologia, 2005. **550**: p. 131-148.
47. Zhu, M.-X., et al., *Reactive iron and its buffering capacity towards dissolved sulfide in sediments of Jiaozhou Bay, China.* Marine Environmental Research, 2012. **80**: p. 46-55.
48. VanCappellen, P. and Y.F. Wang, *Cycling of iron and manganese in surface sediments: A general theory for the coupled transport and reaction of carbon, oxygen, nitrogen, sulfur, iron, and manganese.* American Journal of Science, 1996. **296**(3): p. 197-243.
49. Gamez, V.M., et al., *Anaerobic degradation of citrate under sulfate reducing and methanogenic conditions.* Biodegradation, 2009. **20**(4): p. 499-510.
50. Stams, A.J.M., et al., *Citric acid wastewater as electron donor for biological sulfate reduction.* Applied Microbiology and Biotechnology, 2009. **83**(5): p. 957-963.
51. Reinsch, B.C., et al., *Sulfidation of Silver Nanoparticles Decreases Escherichia coli Growth Inhibition.* Environmental science & technology, 2012. **46**(13): p. 6992-7000.

Table 1: Sediment properties at the freshwater and saltwater nIDDs/DET exposure sites

	Freshwater	Standard Deviation	saltwater	Standard Deviation
Average moisture content (%)	15	2	29	5
Average TOC (%)	17	6	27	4
Particle size (<63, 63-180, >180 µm) (wet sieved)	52, 21, 27 silty sand		82, 2, 16 silt	
Acid Volatile Sulfides (µmol/g)	0.77	0.25	4.37	1.45
pH	7.5	0.2	7.2	0.1

Figure Captions

Figure 1.SEM images of immobilised citrate coated Ag-NPs (A), and PEG coated Ag-NPs (B) on nIDDs

Figure 2. Measured (blue) and fitted (red) Ag K-edge XANES spectra of the PEG-Ag-NPs exposed to different depths of freshwater (A) and saltwater (B) sediment interfaces. Zero represents the sediment-water interface (SWI).

Figure 3. Vertical profiles of dissolved Fe (3A), and Mn (3B) in the saltwater system; and depth profiles (3C) of PEG-Ag-NP speciation in the saltwater system (horizontal dashed lines represent the water-sediment interface)

Figure 4. Vertical profiles of dissolved Fe (3A), and Mn (3B) in the freshwater system; and depth profiles (3C) of PEG-Ag-NP speciation in the freshwater system (horizontal dashed lines represent the water-sediment interface)

Figure 1

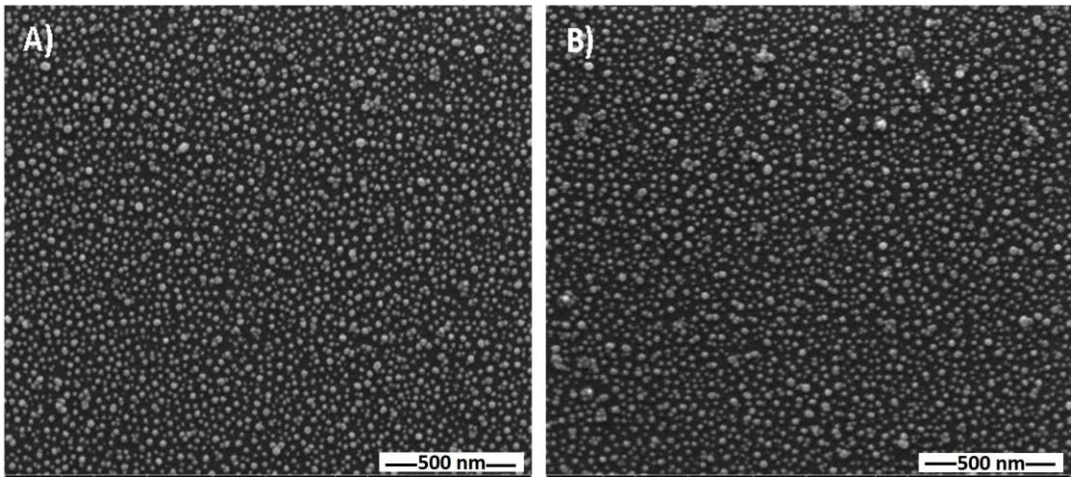
A)
500 nm
B)
500 nm

Figure 2

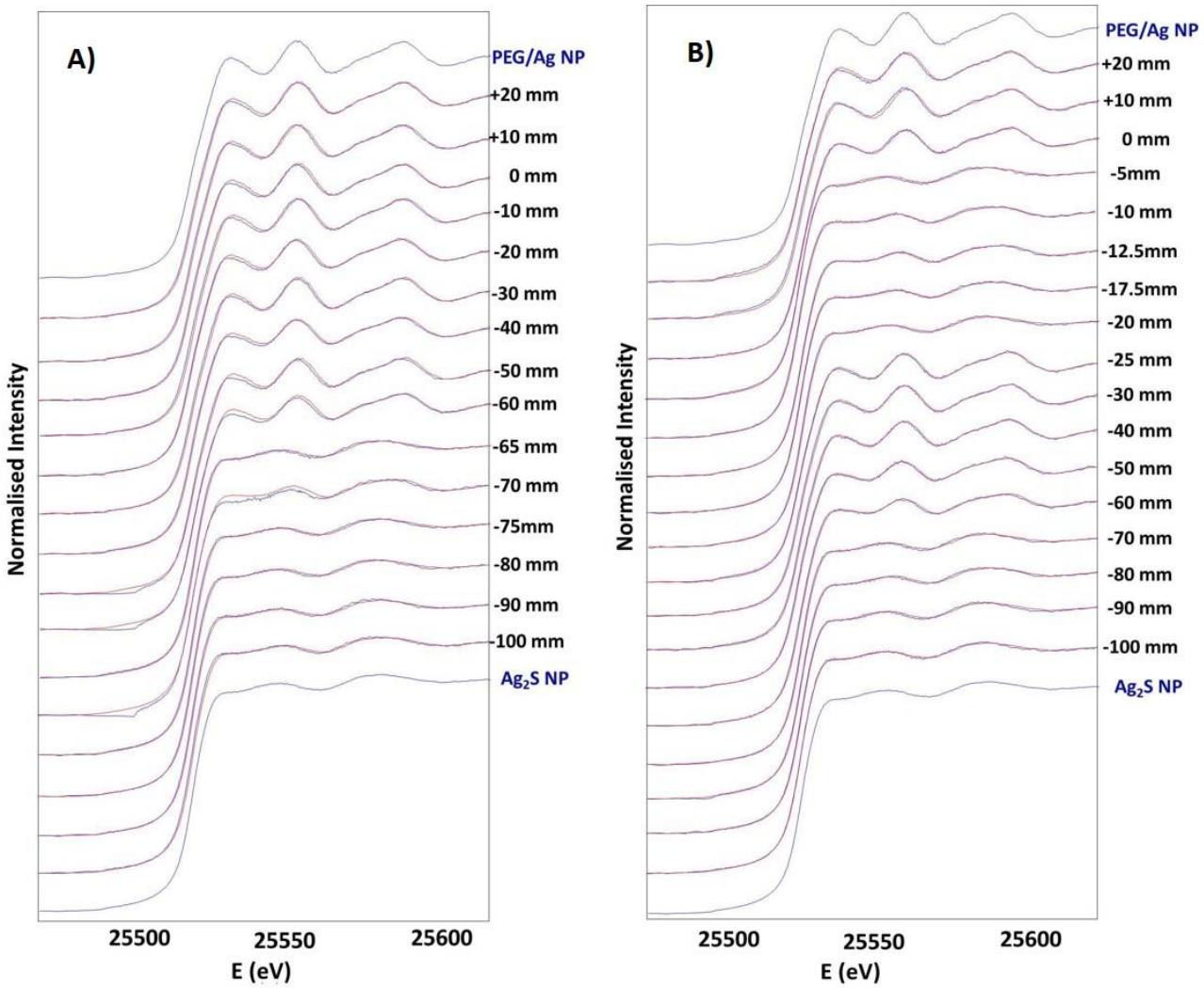
A)
PEG/Ag NP
+20 mm
+10 mm
0 mm
-10 mm
-20 mm
-30 mm
-40 mm
-50 mm
-60 mm
-65 mm
-70 mm
-75mm
-80 mm
-90 mm
-100 mm
Ag2S NP
Normalised Intensity
25500
25550
25600
E (eV)
B)
PEG/Ag NP
+20 mm
+10 mm
0 mm
-5mm
-10 mm
-12.5mm
-17.5mm
-20 mm
-25 mm
-30 mm
-40 mm
-50 mm
-60 mm
-70 mm
-80 mm
-90 mm
-100 mm
Ag2S NP
Normalised Intensity
25500
25550
25600
E (eV)

Figure 3

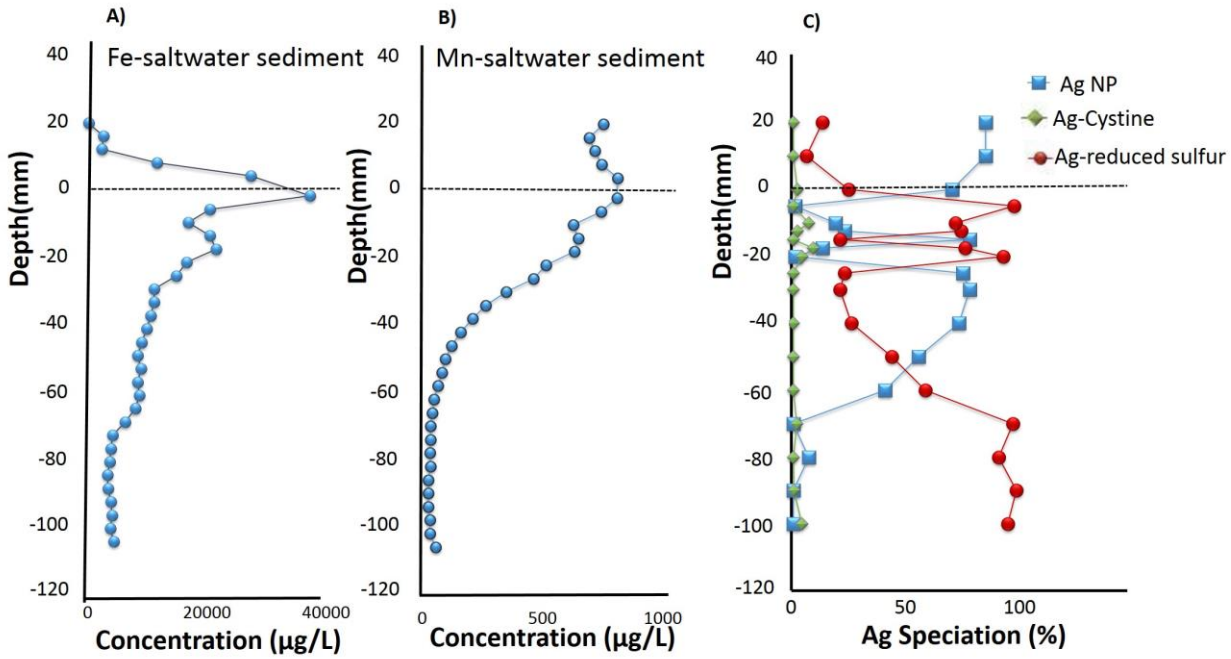

Figure 4

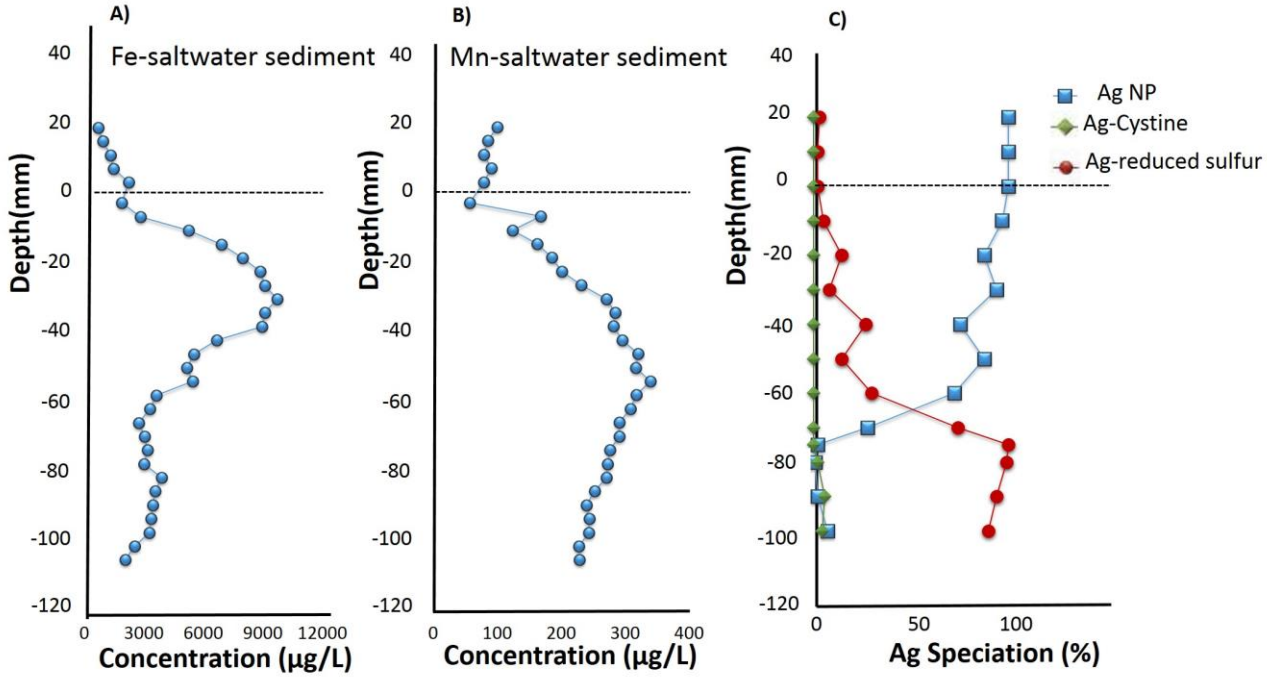

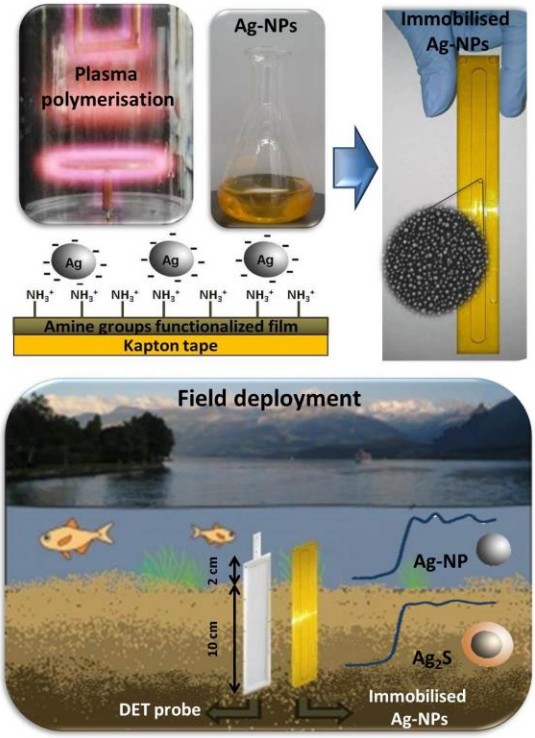
Plasma polymerisation
Ag-NPs
Immobilised Ag-NPs
Ag
Ag
Ag
NH_3^+ NH_3^+ NH_3^+ NH_3^+ NH_3^+ NH_3^+ NH_3^+
Amine groups functionalized film
Kapton tape
Field deployment
2 cm
10 cm
Ag-NP
Ag_2S
DET probe
Immobilised Ag-NPs